AGU PUBLICATIONS

Geophysical Research Letters

RESEARCH LETTERS

10.1002/2017GL076497

Key Points:
- Tidal triggering signal is strong but does not vary systematically in the 2+ years leading up to an eruption
- Tidal triggering signal disappears immediately posteruption
- Tidal triggering variation may not be useful for forecasting eruptions over a 2+ year timescale but might be useful over a longer timescale

Supporting Information:
- Supporting Information S1

Correspondence to:
Y. J. Tan,
yjt@ldeo.columbia.edu

Citation:
Tan, Y. J., Tolstoy, M., Waldhauser, F., & Bohnenstiehl, D. R. (2018). Tidal triggering of microearthquakes over an eruption cycle at 9°50′N East Pacific Rise. *Geophysical Research Letters*, *45*. https://doi.org/10.1002/2017GL076497

Received 18 SEP 2017
Accepted 22 JAN 2018
Accepted article online 29 JAN 2018

Tidal Triggering of Microearthquakes Over an Eruption Cycle at 9°50′N East Pacific Rise

Yen Joe Tan[1], Maya Tolstoy[1], Felix Waldhauser[1], and DelWayne R. Bohnenstiehl[2]

[1] Lamont-Doherty Earth Observatory, Columbia University, Palisades, NY, USA, [2] Department of Marine, Earth, and Atmospheric Sciences, North Carolina State University, Raleigh, NC, USA

Abstract Studies have found that earthquake timing often correlates with tides at mid-ocean ridges and some terrestrial settings. Studies have also suggested that tidal triggering may preferentially happen when a region is critically stressed, making it a potential tool to forecast earthquakes and volcanic eruptions. We examine tidal triggering of ~100,000 microearthquakes near 9°50′N East Pacific Rise recorded between October 2003 and January 2007, which encompasses an eruption in January 2006. This allows us to look at how tidal triggering signal varies over an eruption cycle to examine its utility as a forecasting tool. We find that tidal triggering signal is strong but does not vary systematically in the 2+ years leading up to the eruption. However, tidal triggering signal disappears immediately posteruption. Our findings suggest that tidal triggering variation may not be useful for forecasting mid-ocean ridge eruptions over a 2+ year timescale but might be useful over a longer timescale.

1. Introduction

Studies on whether the periodic stress change of ~1 kPa produced by tidal forcing modulates global earthquake timing have produced conflicting results (e.g., Emter, 1997). Nevertheless, studies have found that earthquake timing correlates with tides for certain environments such as mid-ocean ridges (Bhatnagar et al., 2016; Stroup et al., 2007; Tolstoy et al., 2002; Wilcock, 2001, 2009; Wilcock et al., 2016), shallow thrust faults (Cochran et al., 2004; Tanaka et al., 2002a; Wilcock, 2009), and volcanic regions (McNutt & Beavan, 1984; Rydelek et al., 1988). In subduction zones, studies have also suggested that tidal triggering of earthquakes appears in the years preceding some large earthquakes and disappears after (Tanaka et al., 2002b, 2010, 2012, 2006). Therefore, tidal triggering may happen preferentially when a region is critically stressed (Stroup et al., 2007; Tanaka et al., 2002b, 2010, 2012, 2006; Wilcock et al., 2016), making it a potential tool to forecast earthquakes and volcanic eruptions.

The East Pacific Rise (EPR) is a fast-spreading mid-ocean ridge (>9 cm yr^{-1} at the full spreading rate). Near 9°50′N EPR, a seafloor spreading event in January 2006 ruptured at least 35 km of the ridge axis (Dziak et al., 2009; Tan et al., 2016). The eruption was preceded by 2+ years of increasing seismicity rate (Tolstoy et al., 2006) and was inferred to be largely controlled by the buildup of tectonic stress to a critical level instead of magma overpressure in the underlying magma reservoirs (Tan et al., 2016). Looking at microearthquakes recorded between October 2003 and April 2004, ~2 years before the eruption, Stroup et al. (2007) showed that microearthquake timing at this site correlates with semidiurnal tides, occurring preferentially near times of peak volumetric extensional stress. Subsequent detailed analyses showed systematic spatial variations in earthquake tidal triggering (phase lag relative to times of peak volumetric extensional stress) that is consistent with pore pressure perturbations generated by ocean tidal loading propagating through a hydrothermal system with heterogeneous permeability structure (Crone et al., 2011; Stroup et al., 2009).

Looking at microearthquakes recorded between October 2003 and January 2007, Bhatnagar et al. (2016) subsequently showed that microearthquake timing also correlates with fortnightly tides. While true fortnightly tides have amplitudes of only about 10% that of semidiurnal tides (Agnew, 2007), fortnightly modulations of diurnal and semidiurnal tides have amplitude ranges comparable to semidiurnal tides. Bhatnagar et al. (2016) found that the microearthquakes occurred preferentially during times of increasing volumetric extensional stress before the eruption, and during times of decreasing volumetric extensional stress after the eruption.

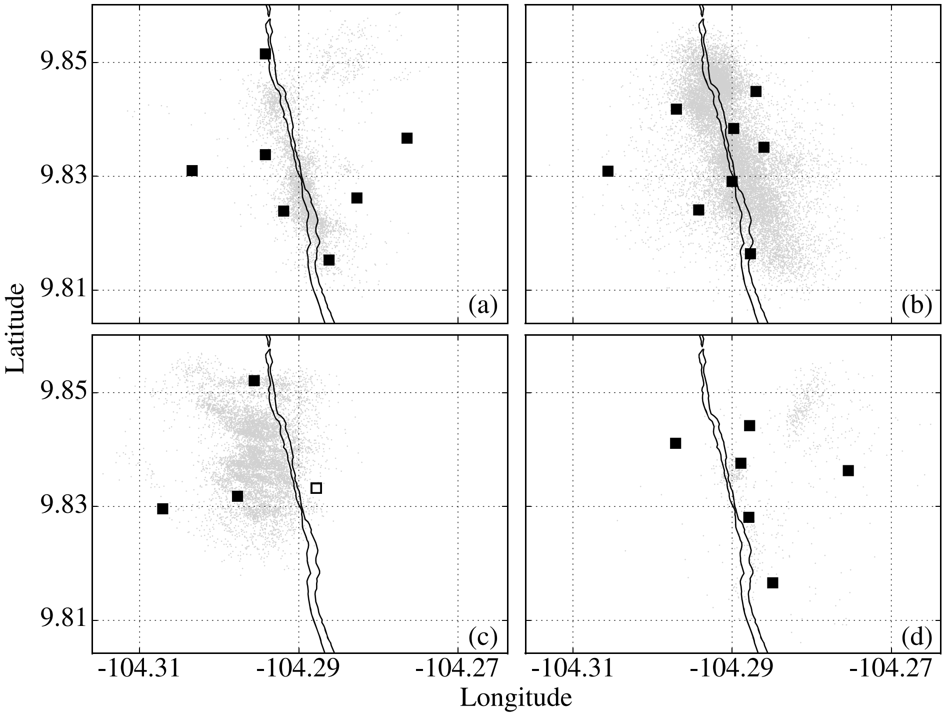

Figure 1. (a–d) Locations of microearthquakes above M_c for deployments 1–4. Station locations are shown as filled black squares. Open black square shows station that only operated from May to July 2005 in deployment 3. Axial summit trough is shown as a thin black line (Soule et al., 2007).

In this study, using ~100,000 microearthquakes recorded from 2+ years before to ~1 year after the eruption, we look at how the microearthquakes' response to semidiurnal tides changes over an eruption cycle at 9°50′N EPR to examine its utility as a forecasting tool.

2. Microearthquakes

From October 2003 to January 2007, up to 12 ocean bottom seismometers (OBSs) were deployed and recovered approximately annually in a 4 × 4 km region near 9°50′N EPR (Tolstoy et al., 2006) (Figure 1). The four deployments were from October 2003 to April 2004, April 2004 to May 2005, May 2005 to April 2006, and April 2006 to January 2007. For deployment 3, because of multiple instrument losses and technical failures, there were four stations operating from May to July 2005, two stations from July to October 2005, and three stations from October 2005 until the end of the deployment (Figure 1). When only two stations were operating, no earthquakes were located.

~100,000 microearthquakes were located for all four deployments using a cross-correlation-based double-difference method (Waldhauser & Ellsworth, 2000; Waldhauser & Tolstoy, 2011). Local magnitudes (M_L) were derived from peak displacement amplitude with attenuation and station correction terms applied. The magnitude of completeness is M_L −0.7 for deployment 1 and M_L −1.0 for deployments 2–4. Approximately 33,000 events are above the magnitude of completeness (M_c), with the largest event of M_L 2.2.

The microearthquakes are inferred to be a result of hydrothermal cracking as well as fracturing from magmatic and tectonic stresses (Tolstoy et al., 2008). Although previous studies in this region have found a range of focal mechanism solutions (normal, thrust, and strike slip) (Sohn et al., 1999; Waldhauser & Tolstoy, 2011), we believe the extension-dominated environment means that the earthquakes likely consist of predominantly crack-opening and/or normal faulting events. The seismicity delineates an along-axis oriented hydrothermal circulation cell and mostly concentrates above the axial magma chamber at 1.5 km depth (Tolstoy et al., 2008; Waldhauser & Tolstoy, 2011). The seismicity rate increased in the 2+ years leading up to an eruption in January 2006 and decreased substantially posteruption (Tan et al., 2016; Tolstoy et al., 2006). Deployment 3 has significantly fewer instruments because many were lost to the lava flow and unrelated instrument failure. Therefore,

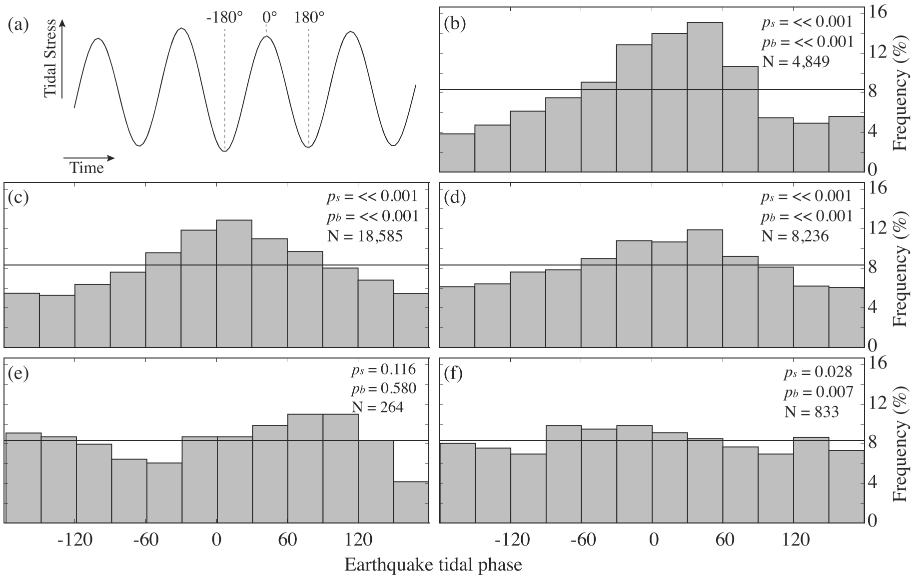

Figure 2. (a) Definition of tidal phase. The phase is 0° at peak tidal stress and ranges from −180° at the preceding minimum to 180° at the subsequent minimum. (b–f) Frequency distributions of earthquake tidal phases for deployment 1, deployment 2, deployment 3 before the eruption, deployment 3 after the eruption, and deployment 4. Only earthquakes above M_c are included. Horizontal black lines mark the expected frequency distribution if the earthquake times are randomly distributed.

earthquakes located in deployment 3 are concentrated west of the ridge axis, reflecting an OBS array that primarily covered the northwest flank of the study area (Figure 1).

3. Tidal Stress and Earthquake Tidal Phase

For the solid Earth tide, we estimate the horizontal strains using the SPOTL software (Agnew, 1997). We then calculate the vertical strain from the horizontal strains using a plane stress condition assuming a Poisson's ratio of 0.25. For the ocean tide, we use the EOT11a ocean tidal model to obtain predicted tidal height for the eight major short-period tidal constituents (K1, K2, M2, N2, O1, P1, Q1, and S2) (Savcenko & Bosch, 2012). We calculate the vertical stress variations from ocean tidal loading directly from the tidal height, assuming a constant water density of 1,025 kg/m^3. We then estimate the horizontal strains from ocean tidal loading using the SPOTL software, which uses a mass-loading Green's function for strain based on the Gutenberg-Bullen Earth model (Agnew, 1997). Finally, we convert strain to stress using *P* and *S* wave velocities as well as density of the top layer of the Gutenberg-Bullen Earth model (Alterman et al., 1961). Since the tidal wavelengths are very long compared to the microearthquake depths of mostly <1.5 km, we assume the stresses modeled at the seafloor are not significantly different from those in the earthquake source region.

The mode of failure of shallow microearthquakes (<1.5 km) in this region is predicted to be tensile or mixed mode (Bohnenstiehl & Carbotte, 2001). Therefore, we focus on variations in volumetric stress, which have estimated amplitudes of ±2.5 kPa, with positive being extensional (Figure S1 in the supporting information). Since our study area is close to an ocean tidal node, tidal stress variation is dominated by the solid Earth tide (Figure S1). We then assign a tidal phase to each earthquake based on its origin time relative to the semidiurnal tides. The phase is 0° at peak tidal stress and ranges from −180° at the preceding minimum to 180° at the subsequent minimum (Figure 2a).

4. Results

For deployments 1–3 before the eruption, frequency distribution of earthquake tidal phases clearly shows that microearthquake timing is modulated by semidiurnal tides (Figure 2). Microearthquakes occur preferentially around times of peak tidal extensional stress (0° phase). We perform the Schuster test to test the null hypothesis that the earthquake times are randomly distributed (Schuster, 1897). We obtain ps of $\ll 0.001$ for deployments 1–3 before the eruption. We also perform the binomial test to estimate the probability p_b

Table 1
Tidal Cycle Statistics for All Deployments

Deployment	N_{enc}	N_{dis}	N_T	p value
1	262	81	343	$\ll 0.001$
2	509	178	687	$\ll 0.001$
3 (before eruption)	213	107	320	$\ll 0.001$
3 (after eruption)	57	47	104	0.378
4	178	142	320	0.050

Note. N_{enc} is the number of tidal cycles with more earthquakes during times of encouraging stress, $-90 < \theta < 90$. N_{dis} is the number of tidal cycles with more earthquakes during times of discouraging stress, $\theta > 90$ and $\theta < -90$. N_T is the sum of N_{enc} and N_{dis}. Only earthquakes above M_c are included.

of observing different numbers of earthquakes during times of encouraging stress, $-90 < \theta < 90$, compared to during times of discouraging stress, $\theta > 90$ and $\theta < -90$, if the earthquake times are randomly distributed. We obtain p_b of $\ll 0.001$ for deployments 1–3 before the eruption. Therefore, both the Schuster and binomial tests support our inference that microearthquake timing is modulated by semidiurnal tides before the eruption. This is further supported by examining the frequency of earthquakes as a function of tidal stress amplitude, which shows that for deployments 1–3 before the eruption, earthquake frequency increases systematically with increasing tidal stress (Figure S2).

For deployment 3 after the eruption, we obtain a p_s of 0.116 and a p_b of 0.580 (Figure 2e). Therefore, we cannot reject the null hypothesis that the earthquake times are randomly distributed. However, this change in p value might be a result of change in sample size since we have significantly fewer earthquakes after the eruption. We randomly draw 264 events (with replacement) from deployment 3 before the eruption and calculate p_s and p_b. This is repeated 1,000 times. We obtain a p_s and a p_b that are smaller than those obtained for deployment 3 after the eruption 96% and 99% of the time. Therefore, this is consistent with the tidal triggering signal disappearing immediately after the eruption. This is further supported by the earthquake frequency not increasing systematically with increasing tidal stress (Figure S2d).

For deployment 4, we obtain a p_s of 0.028 and a p_b of 0.007 (Figure 2f). Frequency distribution of earthquake tidal phases also shows that microearthquakes occur preferentially around times of peak tidal extensional stress (Figure 2f). The earthquake frequency also increases weakly with increasing tidal stress (Figure S2e). These are consistent with tidal triggering signal reappearing within a year after the eruption. However, when we randomly draw 264 events (with replacement) from deployment 4, calculate p_s and p_b, and repeat this 1,000 times, we obtain a p_s and a p_b that are smaller than those obtained for deployment 3 after the eruption only 38% and 85% of the time. Therefore, the reappearance of tidal triggering signal in deployment 4 is not a robust feature.

Earthquakes at mid-ocean ridges are dominated by swarm activities. Therefore, our data set is not amenable to conventional mainshock-aftershock declustering methods. To address the potential effect of swarms on the overall statistics, we look at each semidiurnal tidal cycle and compare the number of earthquakes occurring during times of encouraging stress and discouraging stress. For the null hypothesis that the earthquake times are randomly distributed relative to the semidiurnal tides, this reduces each tidal cycle to the equivalent of one coin flip regardless of the number of earthquakes during the tidal cycle.

For each deployment, we calculate N_{enc}, the number of tidal cycles with more earthquakes during times of encouraging stress, and N_{dis}, the number of tidal cycles with more earthquakes during times of discouraging stress. We exclude tidal cycles where there are equal number of earthquakes during times of encouraging stress and discouraging stress (~9% of cycles). We then perform the binomial test to estimate the probability of observing the given N_{enc}/N_T where $N_T = N_{\mathrm{enc}} + N_{\mathrm{dis}}$, if the earthquake times are randomly distributed. We obtain p values of $\ll 0.001$ for deployments 1–3 before the eruption. This is again consistent with our inference that microearthquake timing is modulated by semidiurnal tides before the eruption.

For deployment 3 after the eruption, we obtain a p value of 0.378 (Table 1). Since the change in p value might be a result of change in sample size, we perform a two-sample z test to evaluate the probability that $N_{\mathrm{enc}}/N_T = 213/320$ (deployment 3 before the eruption) and $N_{\mathrm{enc}}/N_T = 57/104$ (deployment 3 after the eruption)

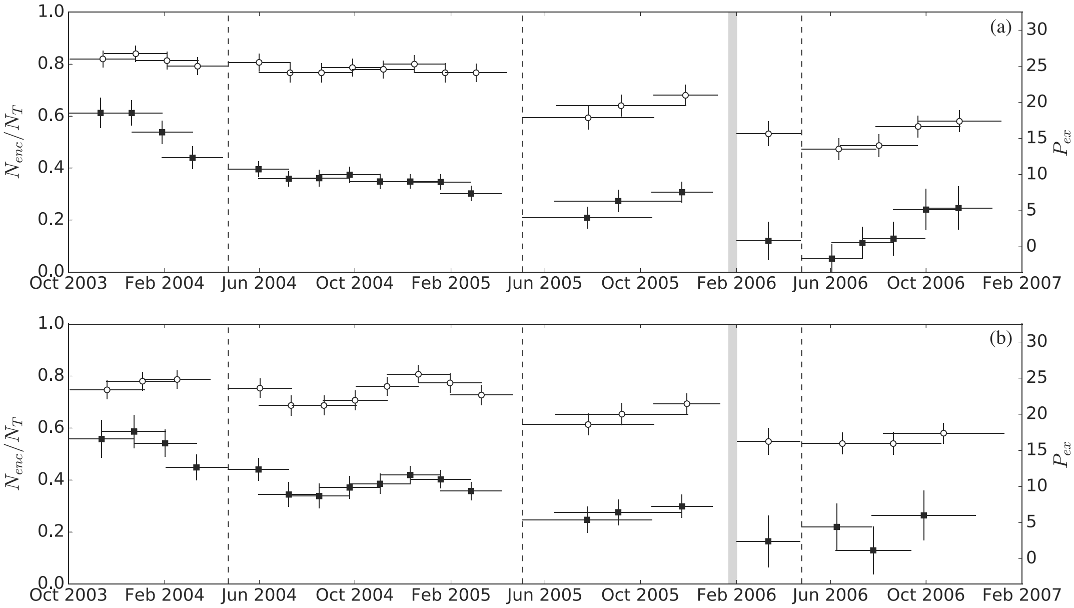

Figure 3. Temporal variation of N_{enc}/N_T (open circles) and P_{ex} (filled squares). Moving windows of 150 semidiurnal tidal cycles, represented by horizontal bars, shifted by 75 tidal cycles. Vertical bars represent 1σ limits estimated based on 1,000 bootstrap samples of the population. Vertical dashed lines mark deployment changes. Gray bar marks the eruption period (Tan et al., 2016). (a) Full catalog. (b) Only earthquakes above M_c.

come from the same population. This yields a z score of 2.2 with a one-tailed probability of 0.015. Therefore, this is consistent with tidal triggering signal disappearing immediately after the eruption. For deployment 4, we obtain a p value of 0.050 (Table 1). Therefore, we cannot reject the null hypothesis that the earthquake times are randomly distributed.

Finally, we examine how the microearthquakes' response to semidiurnal tides varies with time. For each semidiurnal tidal cycle, we calculate the percentage of excess events (P_{ex}) (Cochran et al., 2004):

$$P_{\text{ex}} = \frac{n_{\text{ex}} - \frac{n_T}{2}}{n_T} \times 100, \tag{1}$$

where n_{ex} is the number of earthquakes during times of encouraging stress, $-90<\theta<90$, and n_T is the total number of earthquakes. We then compute the median P_{ex} as well as N_{enc}/N_T for moving windows of 150 semidiurnal tidal cycles with 50% overlap (Figure 3). N_{enc}/N_T should be ~0.5 if the earthquake times are randomly distributed. We use time windows of 150 semidiurnal tidal cycles to minimize the effect of microearthquake timing being modulated by fortnightly tides (Bhatnagar et al., 2016). However, we get similar results when using a smaller time window of 100 semidiurnal tidal cycles, but with larger fluctuations (Figure S3). We examine both the full catalog and the catalog of only earthquakes above M_c to evaluate the temporal variation of P_{ex} and N_{enc}/N_T.

When using the full catalog, N_{enc}/N_T is ~0.8 for both deployments 1 and 2 (Figures 3a and S3a). While N_{enc}/N_T falls to ~0.7 for deployment 3 before the eruption, we think this is likely an effect of changes in earthquake spatial distribution between deployments due to changes in station coverage (Figure 1). Compared to deployments 1 and 2, earthquakes located in deployment 3 are concentrated farther west of the ridge axis (Figure 1). However, in deployment 3, N_{enc}/N_T falls to ~0.6 after the eruption (Figures 3a and S3a). N_{enc}/N_T remains low initially at ~0.6 in deployment 4 but increases toward the end of the deployment. N_{enc}/N_T toward the end of deployment 4 is comparable to that of deployment 3 before the eruption, but smaller than that of deployments 1 and 2 (Figures 3a and S3a). The temporal variation of N_{enc}/N_T is relatively similar when we only examine earthquakes above M_c, but with larger short-term fluctuations (Figures 3b and S3b).

When using the full catalog, P_{ex} decreases with time in both deployments 1 and 2 (Figures 3a and S3a). This could reflect weakening of tidal triggering leading up to the eruption due to changes in the dominant forces driving the microearthquakes (magmatic versus tectonic) (Bhatnagar et al., 2016). However, this is not a robust feature because we do not observe the same trend when we only examine earthquakes above M_c (Figures 3b and S3b). Instead, P_{ex} shows short-term fluctuations which could be due to smaller sample size or temporal changes in earthquake spatial distribution. Regardless, in deployment 3, P_{ex} decreases immediately after the eruption (Figures 3 and S3). P_{ex} remains low initially in deployment 4 but increases toward the end of the deployment. P_{ex} toward the end of deployment 4 is comparable to that of deployment 3 before the eruption, but smaller than that of deployments 1 and 2. The error bars are also larger due to the lower seismicity rate (Figures 3 and S3). The N_{enc}/N_T plot is generally flatter than the P_{ex} plot because while N_{enc}/N_T is expected to correlate with P_{ex}, this relationship levels off at high P_{ex} (Figure S4).

5. Discussion and Conclusions

When examining temporal variation in tidal triggering signal, it is important to consider changes in earthquake spatial distribution. This is because, at least in our study area, susceptibility to tidal triggering as quantified by P_{ex} varies spatially (Figure S5). P_{ex} is larger around 9.82°N, an inferred hydrothermal downflow zone, and smaller around 9.84°N, an inferred hydrothermal upflow zone (Tolstoy et al., 2008). Therefore, especially for deployments 1 and 2 where the differences in array configuration result in an earthquake distribution across areas with very different susceptibility to tidal triggering (Figure S5), temporal variation in P_{ex} may be due to changes in earthquake spatial distribution.

Our analysis suggests that before the eruption near 9°50′N EPR in January 2006 (Tan et al., 2016; Tolstoy et al., 2006), the microearthquake timing is strongly correlated with the semidiurnal tides. This is consistent with previous studies that found tidal triggering of earthquakes at mid-ocean ridges (Bhatnagar et al., 2016; Stroup et al., 2007; Tolstoy et al., 2002; Wilcock, 2001, 2009; Wilcock et al., 2016). The susceptibility of microearthquakes at mid-ocean ridges to tidal triggering may be explained in a few ways. First, the stressing rate due to hydrothermal, magmatic, and tectonic processes may be relatively high, which would lead to a shorter earthquake nucleation time (Dieterich, 1994). A short nucleation time relative to the period of tidal stress variation would result in a system that is more susceptible to tidal triggering (Beeler & Lockner, 2003). However, the occurrence of peak seismicity rate during peak semidiurnal tidal stress suggests that the earthquake nucleation times exceed the semidiurnal tidal period and a nucleation-dominated response instead of a simple threshold failure is expected. In the nucleation-dominated response mode, the response of faults to high-frequency stress change is damped (Beeler & Lockner, 2003). Alternatively, structural heterogeneities at mid-ocean ridges may result in amplification of tidal stresses, such as adjacent to melt lenses, that are significantly greater than the tidal stresses in a homogeneous elastic medium (Dieterich, 1987). Finally, the microearthquakes might be occurring on very weak faults due to the presence of hydrothermal precipitates.

We also observe that the tidal triggering signal disappears immediately posteruption. This is consistent with observations at Axial Seamount where the strong tidal triggering signal in the 4 months leading up to its 2015 eruption weakened after the eruption (Wilcock et al., 2016). The disappearance of the tidal triggering signal immediately posteruption may be explained in a few ways. First, the eruption would have relieved a portion of the accumulated magmatic and tectonic stresses. Therefore, the fault population on average would be farther away from their failure threshold. Alternatively, the relative compression adjacent to the dike might have closed cracks in the surrounding regions, preventing water from flowing as quickly through the hydrothermal circulation cell. This would reduce the stressing rate, which would lead to a longer earthquake nucleation time and weaker susceptibility to tidal triggering (Beeler & Lockner, 2003). However, in the nucleation-dominated response mode, it is unclear from laboratory experiments if the susceptibility to tidal triggering is sensitive to the relative period of earthquake nucleation time and stress oscillation (Beeler & Lockner, 2003).

Finally, we do not observe systematic variation of the tidal triggering signal in the 2+ years leading up to the eruption. This suggests that temporal changes in tidal triggering may not be a useful short-term tool to forecast mid-ocean ridge eruptions. This is supported by Tolstoy et al. (2002) observing strong tidal triggering of earthquakes at Axial Seamount in the summer of 1994, 4 years before it erupted in 1998 (Dziak & Fox, 1999). We also observe that the tidal triggering signal might have reappeared within a year after the eruption. However, due to changes in station coverage between deployments, low seismicity rate after the eruption, and the end of our experiment within a year after the eruption, the duration of recovery to full strength tidal triggering after the eruption is not well constrained by our data. Therefore, it is possible that this recovery takes some years and may thus provide some indication of how far along the eruption cycle the site is. This should hopefully be answered in the near future with data from the Axial Seamount cabled observatory where there is long-term seismic monitoring of an active volcano on a mid-ocean ridge.

Acknowledgments
Y. J. T. thanks Timothy Crone and Heather Savage for fruitful discussions. We thank the captains, crews, and science parties of the R/V Keldysh, R/V *Knorr* and R/V *Atlantis*. This work was supported by NSF grants OCE-0961594 and OCE-1536320. Catalogs used here are available through the Marine Geoscience Data System (http://www.marine-geo.org/portals/gmrt/), in the references cited, or from the authors upon request. Waveform data are available through the IRIS Data Management Center (http://ds.iris.edu/ds/nodes/dmc/).

References

Agnew, D. (2007). Earth tides. *Treatise on Geophysics*, *3*(06), 163–195.

Agnew, D. (1997). NLOADF: A program for computing ocean-tide loading. *Journal of Geophysical Research*, *102*, 5109–5110.

Alterman, Z., Jarosch, H., & Pekeris, C. L. (1961). Propagation of Rayleigh waves in the Earth. *Geophysical Journal International*, *4*, 219–241.

Beeler, N. M., & Lockner, D. A. (2003). Why earthquakes correlate weakly with the solid Earth tides: Effect of periodic stress on the rate and probability of earthquake occurrence. *Journal of Geophysical Research*, *108*(B8), 2391. https://doi.org/10.1029/2001JB001518

Bhatnagar, T., Tolstoy, M., & Waldhauser, F. (2016). Influence of fortnightly tides on earthquake triggering at the East Pacific Rise at 9°50′N. *Journal of Geophysical Research: Solid Earth*, *121*, 1262–1279. https://doi.org/10.1002/2015JB012388

Bohnenstiehl, D. R., & Carbotte, S. M. (2001). Faulting patterns near 19°30′S on the East Pacific Rise: Fault formation and growth at a superfast spreading center. *Geochemistry, Geophysics, Geosystems*, *2*(9), 1056. https://doi.org/10.1029/2001GC000156

Cochran, E. S., Vidale, J. E., & Tanaka, S. (2004). Earth tides can trigger shallow thrust fault earthquakes. *Science*, *306*, 1164–1166. https://doi.org/10.1126/science.1103961

Crone, T. J., Tolstoy, M., & Stroup, D. F. (2011). Permeability structure of young ocean crust from poroelastically triggered earthquakes. *Geophysical Research Letters*, *38*, L05305. https://doi.org/10.1029/2011GL046820

Dieterich, J. H. (1994). A constitutive law for rate of earthquake production and its application to earthquake clustering. *Journal of Geophysical Research*, *99*, 2601–2618.

Dieterich, J. H. (1987). Nucleation and triggering of earthquake slip: Effect of periodic stress. *Tectonophysics*, *144*, 127–139.

Dziak, R. P., Bohnenstiehl, D. R., Matsumoto, H., Fowler, M. J., Haxel, J. H., Tolstoy, M., & Waldhauser, F. (2009). January 2006 seafloor-spreading event at 9°50′N, East Pacific Rise: Ridge dike intrusion and transform fault interactions from regional hydroacoustic data. *Geochemistry, Geophysics, Geosystems*, *10*, Q06T06. https://doi.org/10.1029/2009GC002388

Dziak, R. P., & Fox, C. G. (1999). Long-term seismicity and ground deformation at Axial Volcano, Juan de Fuca Ridge. *Geophysical Research Letters*, *26*, 3641–3644.

Emter, D. (1997). Tidal triggering of earthquakes and volcanic events. In S. Bhattacharji (Ed.), *Tidal Phenomena* (pp. 293–309). New York: Springer.

McNutt, S. R., & Beavan, R. J. (1984). Patterns of earthquakes and the effect of solid earth and ocean load tides at Mount St. Helens prior to the May 18, 1980, eruption. *Journal of Geophysical Research*, *89*, 3075–3086.

Rydelek, P. A., Davis, P. M., & Koyanagi, R. Y. (1988). Tidal triggering of earthquake swarms at Kilauea Volcano, Hawaii. *Journal of Geophysical Research*, *93*, 4401–4411.

Savcenko, R., & Bosch, W. (2012). EOT11a—Empirical ocean tide model from multi-mission satellite altimetry (DGFI Report No. 89). München: Deutsches Geodätisches Forschungsinstitut (DGFI).

Schuster, A. (1897). On lunar and solar periodicities of earthquakes. *Proceedings of the Royal Society of London*, *61*, 455–465.

Sohn, R. A., Hildebrand, J. A., & Webb, S. C. (1999). A microearthquake survey of the high-temperature vent fields on the volcanically active East Pacific Rise (9°50′N). *Journal of Geophysical Research*, *104*, 25,367–25,377.

Soule, S. A., Fornari, D. J., Perfit, M. R., & Rubin, K. H. (2007). New insights into mid-ocean ridge volcanic processes from the 2005–2006 eruption of the East Pacific Rise, 9°46′N–9°56′N. *Geology*, *35*, 1079–1082.

Stroup, D. F., Bohnenstiehl, D. R., Tolstoy, M., Waldhauser, F., & Weekly, R. T. (2007). Pulse of the seafloor: Tidal triggering of microearthquakes at 9°50′N East Pacific Rise. *Geophysical Research Letters*, *34*, L15301. https://doi.org/10.1029/2007GL030088

Stroup, D. F., Tolstoy, M., Crone, T. J., Malinverno, A., Bohnenstiehl, D. R., & Waldhauser, F. (2009). Systematic long-axis tidal triggering of microearthquakes observed at 9°50′N East Pacific Rise. *Geophysical Research Letters*, *36*, L18302. https://doi.org/10.1029/2009GL039493

Tan, Y. J., Tolstoy, M., Waldhauser, F., & Wilcock, W. S. D. (2016). Dynamics of a seafloor-spreading episode at the East Pacific Rise. *Nature*, *540*, 261–265.

Tanaka, S., Ohtake, M., & Sato, H. (2002a). Evidence for tidal triggering of earthquakes as revealed from statistical analysis of global data. *Journal of Geophysical Research*, *107*(B10), 2211. https://doi.org/10.1029/2001JB001577

Tanaka, S., Ohtake, M., & Sato, H. (2002b). Spatio-temporal variation of the tidal triggering effect on earthquake occurrence associated with the 1982 South Tonga earthquake of *Mw* 7.5. *Geophysical Research Letters*, *29*(16), 3134. https://doi.org/10.1029/2002GL015386

Tanaka, S., Sato, H., Matsumura, S., & Ohtake, M. (2006). Tidal triggering of earthquakes in the subducting Philippine Sea plate beneath the locked zone of the plate interface in the Tokai region, Japan. *Tectonophysics*, *417*, 69–80. https://doi.org/10.1016/j.tecto.2005.09.013

Tanaka, S. (2010). Tidal triggering of earthquakes precursory to the recent Sumatra megathrust earthquakes of 26 December 2004 (*Mw*9.0), 28 March 2005 (*Mw*8.6), and 12 September 2007 (*Mw*8.5). *Geophysical Research Letters*, *37*, L02301. https://doi.org/10.1029/2009GL041581

Tanaka, S. (2012). Tidal triggering of earthquakes prior to the 2011 Tohoku-Oki earthquake (*Mw*9.1). *Geophysical Research Letters*, *39*, L00G26. https://doi.org/10.1029/2012GL051179

Tolstoy, M., Cowen, J. P., Baker, E. T., Fornari D. J., Rubin, K. H., Shank, T. M., et al. (2006). A seafloor spreading event captured by seismometers. *Science*, *314*, 1920–1922. https://doi.org/10.1126/science.1133950

Tolstoy, M., Vernon, F. L., Orcutt, J. A., & Wyatt, F. K. (2002). Breathing of the seafloor: Tidal correlations of seismicity at Axial Volcano. *Geology*, *30*, 503–506.

Tolstoy, M., Waldhauser, F., Bohnenstiehl, D. R., Weekly, R. T., & Kim, W.-Y. (2008). Seismic identification of along-axis hydrothermal flow on the East Pacific Rise. *Nature*, *451*, 181–184. https://doi.org/10.1038/nature06424

Waldhauser, F., & Ellsworth, W. L. (2000). A double-difference earthquake location and algorithm: Method and application to the northern Hayward Fault, California. *Bulletin of the Seismological Society of America*, *90*, 1353–1368. https://doi.org/10.1785/0120000006

Waldhauser, F., & Tolstoy, M. (2011). Seismogenic structure and processes associated with magma inflation and hydrothermal circulation beneath the East Pacific Rise at 9°50′N. *Geochemistry, Geophysics, Geosystems*, *12*, Q08T10. https://doi.org/10.1029/2011GC003568

Wilcock, W. S. D. (2001). Tidal triggering of microearthquakes on the Juan de Fuca Ridge. *Geophysical Research Letters*, *28*, 3999–4002.

Wilcock, W. S. D. (2009). Tidal triggering of earthquakes in the Northeast Pacific Ocean. *Geophysical Journal International*, *179*, 1055–1070.

Wilcock, W. S. D., Tolstoy, M., Waldhauser, F., Garcia, C., Tan, Y. J., Bohnenstiehl, D. R., et al. (2016). The 2015 eruption of Axial Seamount: Seismic constraints on caldera dynamics. *Science*, *354*(6318), 1395–1399.

Supporting Information for
"Tidal triggering of microearthquakes over an eruption cycle at 9°50'N East Pacific Rise"

Yen Joe Tan[1], **Maya Tolstoy**[1], **Felix Waldhauser**[1], **and DelWayne R. Bohnenstiehl**[2]

[1]Lamont-Doherty Earth Observatory of Columbia University, Palisades, New York 10964, USA.

[2]Department of Marine, Earth, and Atmospheric Sciences, North Carolina State University, Raleigh, NC 27695, USA.

Contents

1. Figure S1

   Volumetric stress from solid Earth tide (red), ocean tidal loading (blue), and the combined effect of solid Earth and ocean tide (black).

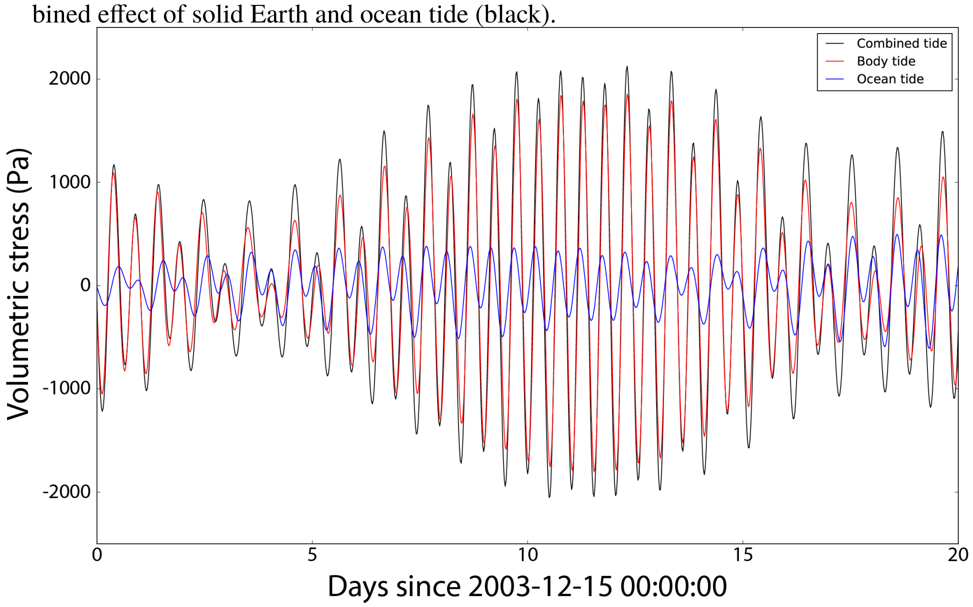

2. Figure S2

   (a-e) The normalized frequency of earthquakes (number per hour divided by the maximum number per hour) as a function of tidal volumetric stress in 0.5 kPa bins for deployment 1, deployment 2, deployment 3 before the eruption, deployment 3 after the eruption, and deployment 4 respectively. Dashed lines show the mean normalized frequency of earthquakes. Only earthquakes above M_c are included.

Corresponding author: Yen Joe Tan, `yjt@ldeo.columbia.edu`

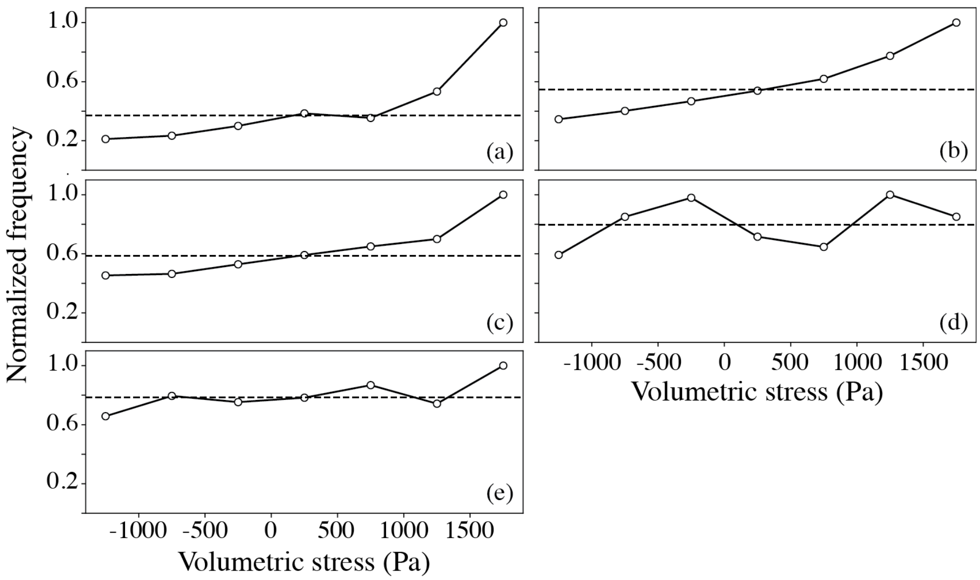

3. Figure S3

   Temporal variation of N_{enc}/N_T (open circles) and P_{ex} (filled squares). Moving windows of 100 semidiurnal tidal cycles, represented by horizontal bars, shifted by 50 tidal cycles. Vertical bars represent 1σ limits estimated based on 1,000 bootstrap samples of the population. Vertical dashed lines mark deployment changes. Gray bar marks the eruption period [*Tan et al.*, 2016]. (a) Full catalog. (b) Only earthquakes above M_c.

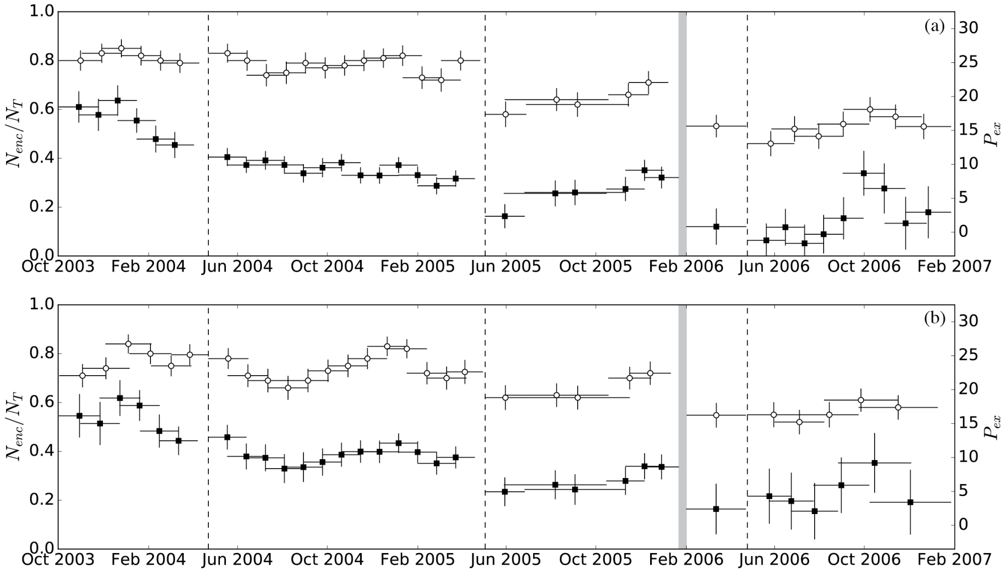

4. Figure S4

Relationship between N_{enc}/N_T and P_{ex} when events are independent and randomly distributed in time. For each synthetic run, we generate a catalog of 1,000 events randomly distributed over 100 tidal cycles, with a prescribed P_{ex} over the whole time period. We then calculate the N_{enc}/N_T. We do this for a range of prescribed P_{ex}. The plots shows that N_{enc}/N_T and P_{ex} are generally correlated, but N_{enc}/N_T levels off at high P_{ex}. Grey bar marks the range of P_{ex} observed in our study (Figure 3 and S3).

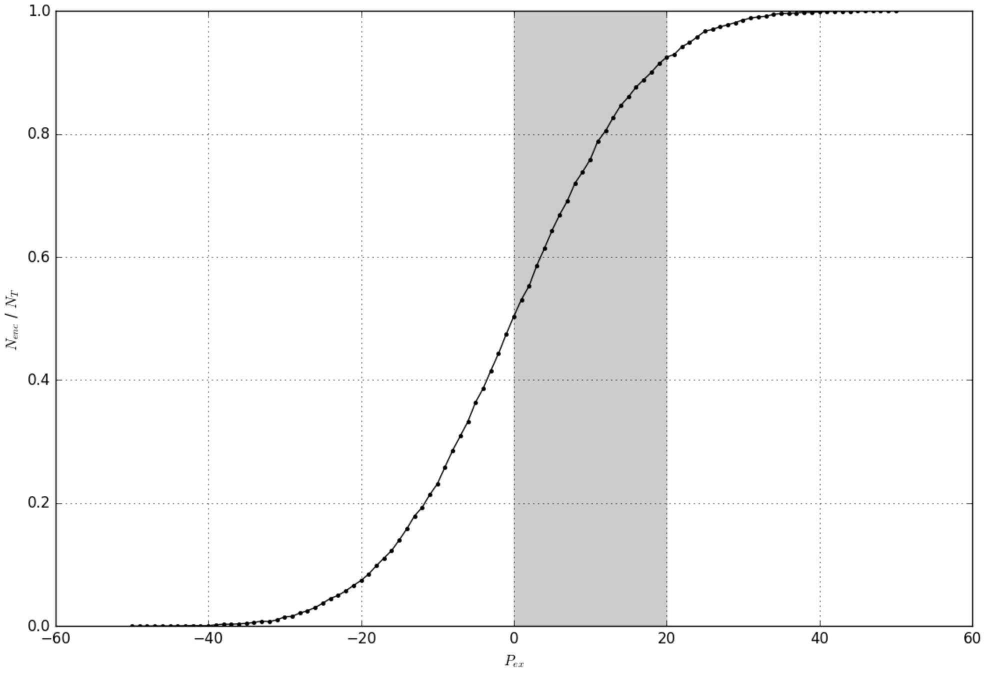

5. Figure S5

Along-axis 2D spatial variation of (a-d) earthquake distribution for deployment 1 to 4 and (e-h) P_{ex} for deployment 1 to 4. Only earthquakes above M_c were included. For P_{ex}, only grids with at least 10 events are included.

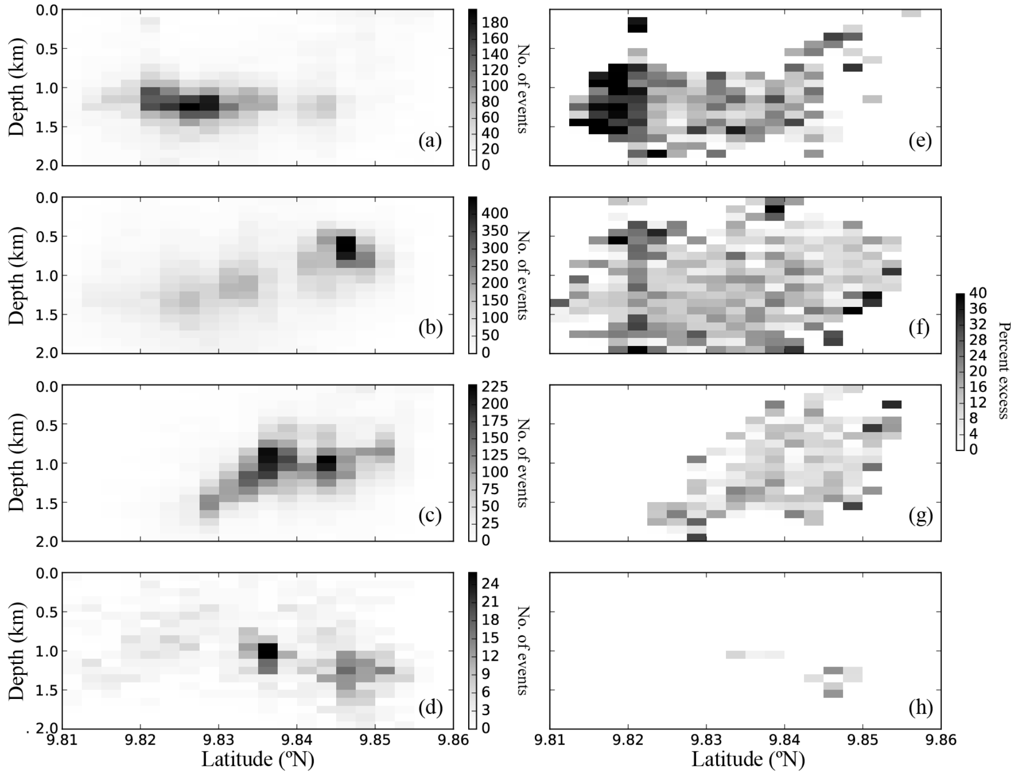

References

Tan, Y. J., M. Tolstoy, F. Waldhauser, and W. S. D. Wilcock (2016), Dynamics of a seafloor-spreading episode at the East Pacific Rise, *Nature, 540*, 261–265.